

The effect of riboflavin on the microbiologically influenced corrosion of X80 Pipeline Steel by *Escherichia Coli*

Shisen Yan¹, Yingqian Zhang⁵, Lei Fu^{1,3*}, Li Lin^{2,4*}, Sheng Lai¹, Zhengguo Wang^{1,2}, Mingxing Tan¹, Jieshuang Mu¹, Yanbing Guan¹

¹ School of Mechanical Engineering, Sichuan University of Science & Engineering, Zigong 643000, People's Republic of China

² Sichuan Provincial Key Lab of Process Equipment and Control, Zigong 643000, People's Republic of China

³ Failure Mechanics and Engineering Disaster Prevention, Key Lab of Sichuan Province, Sichuan University, Chengdu, 610065, People's Republic of China

⁴ College of Materials and Chemistry and Chemical Engineering, Chengdu University of Technology, Chengdu 610059, People's Republic of China

⁵ School of Civil Engineering, Sichuan University of Science & Engineering, Zigong 643000, People's Republic of China

*E-mail: kunmingfulei@126.com and linli1031@126.com

Received: 1 June 2022 / Accepted: 8 August 2022 / Published: 10 September 2022

Endogenous electron shuttling riboflavin (RF) was used as a carrier to investigate the *Escherichia coli* (*E. coli*) corrosion effect in X80 pipeline steel by cyclic voltammetry (CV), corrosion weight loss, electrochemical testing, scanning electron microscopy (SEM), energy spectrum analysis (EDS) and diffraction of x-rays (XRD) analysis. The CV results showed that the *E. coli* bacterium and its metabolites did not exhibit electroactivity. After adding RF, the redox peak appeared in the system, indicating that *E. coli* can use RF for extracellular electron transfer. The corrosion weight loss rate showed that the corrosion rate of X80 pipeline steel of the *E. coli* + 20 ppm RF system is about twice that of the *E. coli* system. XRD test results showed that RF did not change the corrosion pathway of *E. coli* and only affected the corrosion process of *E. coli*. Electrochemical tests showed that the corrosion current density of the *E. coli* + 20 ppm RF system was 1.5 times that of the *E. coli* system. Therefore, *E. coli* accelerates the corrosion of X80 pipeline steel through RF for extracellular electron transfer.

Keywords: X80 pipeline steel; *Escherichia coli*; Riboflavin; Electron shuttle

1. INTRODUCTION

With the rapid economic development of China and the increasing national income, the demand for oil and natural gas is growing, and the oil and gas transportation pipeline network is expanding. In

2020, domestic oil and gas pipelines reached 144,000km. The service reliability of pipeline steel directly affects the safety performance of oil transportation pipelines [1,2]. However, the pipeline service environment is complex, and microbes play an important role in ecological improvement and repair and inducing microbial corrosion of the pipelines [3-6]. Most microbial growth and metabolic activity occur on the pipeline's surface and through electron transfer with the metallic materials of the channel [7,8], triggering redox reactions and leading to corrosion failure of the metallic materials of the pipeline in service [9,10].

Studies suggest that the essence of the redox reaction between microorganisms and pipeline metals is the electron transfer between metals and microorganisms caused by microbial metabolic activity [11-13]. Based on the possible existence of an electron transfer mechanism in the biological cathode inverse to the biological anode [14], Xu et al. [15-17] first introduced "extracellular electron transfer" into microbial corrosion studies, suggesting that electro-active microorganisms could influence metal corrosion through electron shuttles. Zhou et al. [18] proposed that flavins can act as electron shuttles, allowing microorganisms far from the metal to get electrons and accelerating corrosion. Zhang et al. [19] found that electron shuttles such as flavins and riboflavin (RF) would increase pitting depth and promote corrosion of metals. Therefore, studying the effect of electron shuttle on corrosion is of great significance to re-understand pipeline corrosion and explore pipeline corrosion protection.

There are few studies on the effects of electron shuttles on the corrosion of metallic materials. This paper investigated the RF effects on the *E. coli* corrosion of X80 pipeline steel through microscopic morphological observation combined with electrochemical testing and other methods. The provided data support investigating the extracellular electron transfer process and the *E. coli* electron transfer mechanism.

2. EXPERIMENTAL METHOD

2.1. Experimental materials and culture medium

X80 pipeline steel is mainly acicular ferrite (AF) and granular ferrite (GF) with an M-A organization in acicular/granular ferrite and ferrite. The chemical composition and metallographic organization of the X80 pipeline steel are shown in Table 1 and Fig 1. Two sizes of X80 pipeline steel were used, the large size of 50 mm × 25 mm × 3 mm sheets for weight loss rate analysis and the small size of 15 mm × 10 mm × 3 mm sheets for corrosion morphology analysis. In a processing size of 10 mm × 10 mm × 10 mm, Cu wire was soldered on the top surface by cutting a hole, except for the working surface. The surface was sealed with epoxy resin made of the electrochemical working electrode. The sheets and electrochemical working electrodes were sequentially polished with 1200# and 60# sandpaper to make the scratches in the same direction. The sheets were degreased with acetone, disinfected with 75% alcohol, blown dry, and placed into a dry dish to be used. The sheets were put into the ultra-clean bench for 30 minutes after the ultraviolet lamp before each use.

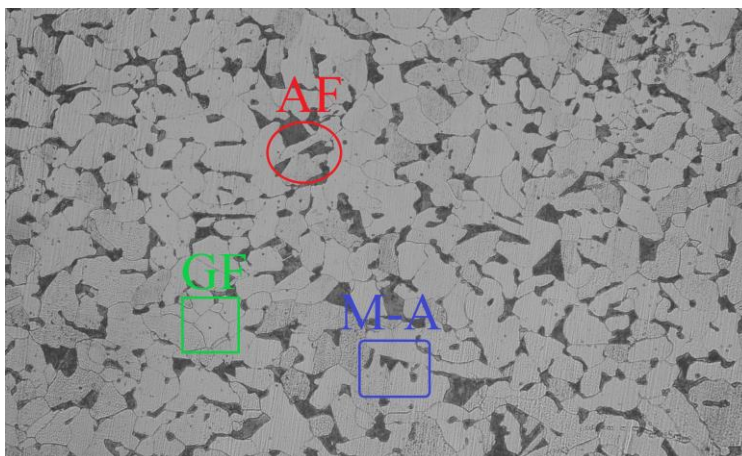


Figure 1. Metallographic drawing of the uncorroded X80 pipeline steel

Table 1. Chemical composition of X80 pipeline steel (wt.%)

Element	C	Si	Mn	P	S	Ni	Cu	Mo	N	Nb	Al	Ti	Cr	Fe
wt/%	0.07	0.215	1.8	0.014	0.0008	0.165	0.2	0.18	0.002	0.1	0.02	0.01	0.25	other

E. coli was cultured in a broth medium containing peptone 5.0 g, beef extract 3.0 g, and NaCl 5.0 g, diluted in distilled water 1 L. The pH value of the culture medium was adjusted to 7.0 with 2.5 mol/L NaOH solution. The culture medium was placed in a vertical autoclave and sterilized at 121° for 20 minutes.

2.2. Microbial inoculation

The culture medium was sterilized, cooled, placed on the ultra-clean bench, and sanitized with an ultraviolet lamp for 30 minutes. The *E. coli* was provided by the China Center of Industrial Culture Collection (CICC) (No. 23429). *E. coli* was inoculated at 5%, then placed in a constant-temperature shaker incubator at 36°C with a shaker speed of 90 r/min.

2.3. Escherichia coli electroactivity test

E. coli electroactivity was tested by cyclic voltammetry (CV) using a three-electrode system (Chenhua CHI660). The reference electrode was a saturated calomel electrode, the auxiliary electrode was a platinum electrode, and the working electrode was a glassy carbon electrode (GCE) with a functional area of 3 mm in diameter. The CV curve of 1×10^{-3} mol/L $K_3Fe(CN)_6$ solution was tested in 0.2 mol/L KNO_3 with a scan rate of 10 mV/s and a sweeping range of 0.5 ~ -0.1V. The peak potential of the measured curve should be between 80 mV and 120 mV. The anodic peak potential of the CV curve is 260 mV, the cathodic peak potential is 164 mV, and the peak potential difference of the CV curve is 96 mV, as shown in Fig 2.

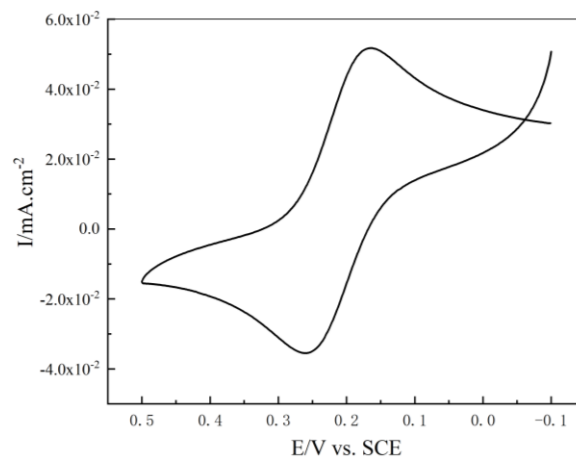


Figure 2. Cyclic voltammogram of GCE in $K_3Fe(CN)_6$ solution

Microbial electro-active tests were performed in different solutions: phosphate buffered saline (PBS) (2.5 g NaCl, 0.0625 g KCl, 0.45 g $Na_2HPO_4 \cdot 12H_2O$, 0.075 g KH_2PO_4 , 20 mM D-glucose in 1L distilled water), PBS + 5% *E. coli* suspension, *E. coli*, *E. coli* + N_2 , *E. coli* + 10 ppm RF, *E. coli* + 20 ppm RF, *E. coli* + 30 ppm RF, *E. coli* + 40 ppm RF, *E. coli* + 50 ppm RF and *E. coli* + 100 ppm RF. The CV scan voltage range was -1 ~ 0V, and the scan rate was 10 mv/s.

2.4. Corrosion weight loss

To analyze the effect of *E. coli* on the X80 pipeline steel corrosion under the action of RF, the test was set up with the blank system, RF system, *E. coli* system, and *E. coli* + RF system. The culture medium was changed every five days, and each group of three large-size sheets was subjected to a 20d corrosion weight loss test. The sheets were weighed and marked before the test. Each group of two small-sized sheets was subjected to 5d, 10d, 15d, and 20d immersion tests for corrosion product analysis and morphology observation. The small-sized sheets of *E. coli* system and *E. coli* + RF systems were removed after predetermined immersion times, cured with 5% glutaraldehyde in PBS for three hours, sequentially dehydrated with 70%, 80%, 90%, and 100% alcohol for 10 minutes each, and blow-dried. The small-sized sheets of the blank and the RF systems were removed after predetermined immersion times, washed with deionized water and alcohol and blow-dried. The sheet's surface morphology was observed using a scanning electron microscope (VEGA), and EDS analyzed the elements of corrosion products on the surface of the sheets. The corrosion morphology was observed after the corrosion products were removed from the sheet's surface. The corrosion products were collected, and corrosion product phase composition was analyzed by an X-ray diffractometer (Bruker D2-PHASER).

2.5. Electrochemical test

Before the test, the electrochemical devices were autoclaved under the same conditions as in section 2.1. The working electrodes, saturated calomel electrodes, and platinum electrodes were first

sterilized with medical alcohol for two hours, placed on an ultra-clean bench, and sanitized with an ultraviolet lamp for 30 minutes. The test was divided into four systems: a) blank system; b) RF system; c) *E. coli* system; d) *E. coli* + RF system. The tests were performed using the Solartron 1287+1260A electrochemical workstation, UK, with saturated calomel electrode as reference electrode, X80 pipeline steel as the working electrode, and platinum electrode as the auxiliary electrode. The open-circuit potential (OCP) and AC impedance spectroscopy (EIS) were measured at 1 d, 2 d, 3 d, 4 d, 5 d, 6 d, and 7 d. Polarization curve measurement was performed on day 7. Electrochemical tests were performed for OCP for 30 minutes and EIS after the OCP stabilized. The perturbation voltage was a sinusoidal signal of 10 mV, and the test frequency range was 10 mHz to 10 KHz. The polarization range was -0.25 V ~ 0.25 V (VS OCP), and the scan rate was 1 mV/s. The EIS was fitted using the ZsimpWin software, and self-corrosion potential and polarization curve test results were fitted with CVIEW2.

3. RESULTS AND DISCUSSION

3.1. Electroactivity analysis of *E. coli*

3.1.1. Electroactivity analysis of *E. coli* in different systems

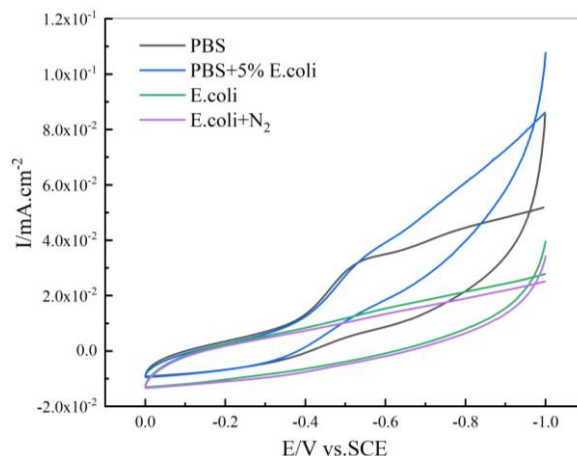


Figure 3. Cyclic voltammograms of GCE in different systems (PBS, PBS + 5% *E. coli*, *E. coli*, *E. coli* + N₂)

E. coli was centrifuged at high speed, and the *E. coli* bacterial pellet was resuspended in PBS at a 5% ratio to explore whether *E. coli* had electro-active properties, PBS without *E. coli* bacterial suspension was used as a blank control test. As shown in Fig 3, there was no redox peak in the *E. coli* system, indicating that *E. coli* was not electro-active.

Because *E. coli* is a facultative anaerobe, to investigate the *E. coli* electroactivity changed under different metabolic conditions, the CV test was performed after 1 h of N₂ deoxygenation in the culture medium, and the results are shown in Fig 3. As shown in Fig 3, no redox peaks appeared in the *E. coli* system in aerobic and anaerobic conditions, indicating that the metabolites were not electro-active under either condition.

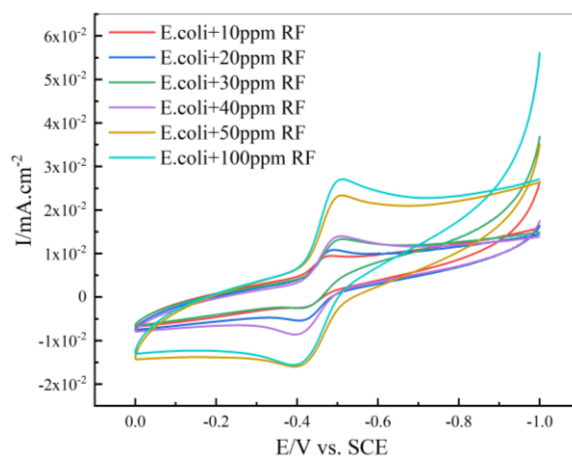
3.1.2. Effect of the electron shuttle RF on the electro-active of *E. coli*

Figure 4. Cyclic voltammograms of GCE in different RF concentrations (10ppm RF, 20ppm RF, 30ppm RF, 40ppm RF, 50ppm RF, 100ppm RF)

To investigate the effect of different concentrations of RF on the electro-active of *E. coli*, 10, 20, 30, 40, 50, and 100 ppm RF were added to the *E. coli*-containing medium for CV testing and the results are shown in Fig 4. This is consistent with Zhang et al. who suggested that the electron carrier RF enhances the biofilm electroactivity of microorganisms [20]. Theoretically, the redox peak height and symmetry of the CV curve determine the reversibility degree of electro-active substances on the electrode surface. The potential difference (ΔE_p) of the redox peak for the reversible reaction is $0.059/nV$ (where n indicates the number of transferred electrons), and the peak current ratio (I_{pa}/I_{pc}) between the oxidation and reduction peaks is close to 1. As shown in Fig 4, at 10 ppm RF, a cathodic peak appeared at -0.484 V, indicating that the system contained redox components and was involved in the electron transfer between electrodes. At 20 ppm RF, the anodic and cathodic peaks were at -0.489 V and -0.401 V, respectively, ΔE_p was about 0.088 V, and I_{pa}/I_{pc} was about 1.15 was a quasi-reversible process. At 30 ppm RF, the anodic and cathodic peaks were located at -0.512 V and -0.399 V, respectively, ΔE_p was about 0.113 V, and I_{pa}/I_{pc} was about 1.1, which was a quasi-reversible reaction. At 40 ppm RF, the anodic and cathodic peaks were located at -0.510 V and -0.396 V, respectively, ΔE_p was about 0.111 V, and I_{pa}/I_{pc} was about 1.07, which was a quasi-reversible reaction. At 50 ppm RF, the anodic and cathodic peaks were located at -0.513 V and -0.399 V, respectively, ΔE_p was about 0.114 V, and I_{pa}/I_{pc} was about 1.56, which was a quasi-reversible reaction. At 100 ppm RF, the anodic and cathodic peaks located at -0.513 V and -0.390 V, ΔE_p was about 0.123 V, and I_{pa}/I_{pc} was about 1.53 was a quasi-reversible reaction. The redox peaks appeared in the CV curves at 20, 30, 40, 50, and 100 pm RF with a sweep rate of 10 mV/s, indicating that RF was involved in the electron transfer between *E. coli* and the electrode, and the peak current increase with RF concentration. The closest quasi-reversible reaction to the reversible electrochemical reaction was at an RF concentration of 20 ppm.

As shown in Fig 5, the *E. coli* + 20 ppm RF system was tested at different scan rates. The reduction peak positively shifted, and the oxidation peak remained negative with the scan rate increase.

The fitting results of the $V^{1/2}$ and peak current test data as shown in Fig 6. At 20 ppm RF, the peak current had an excellent linear correlation with $V^{1/2}$, following Randles Sevcik's controlled diffusion-reaction equation (1), indicating that the RF redox process dominated the diffusion control [21,22].

$$i_{pea} = (2.69 \times 10^5)n^{3/2}AD_0^{1/2}C_0^*v^{1/2} \quad (1)$$

In the formula, i_{pea} is the peak current, n is the number of electron transfers for redox, A is the electrode area, D_0 is the diffusion coefficient of RF ions, C_0^* is the initial mass concentration of RF, and v is the sweep rate of CV curve test.

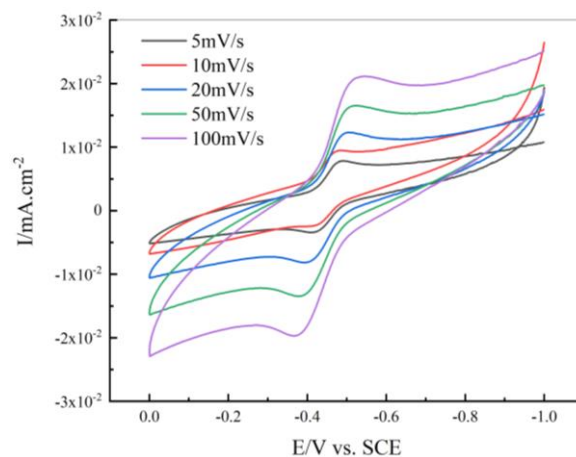


Figure 5. Cyclic voltammograms of GCE in *E. coli* + 20 ppm RF system at different scan rates (5 mV/s, 10 mV/s, 20 mV/s, 50 mV/s, 100 mV/s)

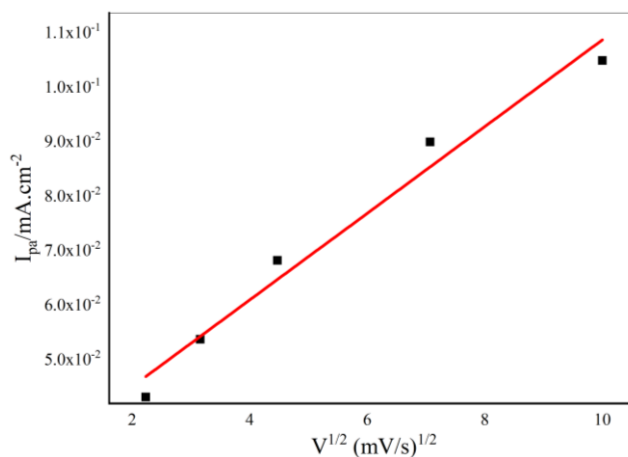


Figure 6. The anodic peak current as a function of the scan rate for GCE in *E. coli* + 20 ppm RF system

3.2. Corrosion weight loss rate

The corrosion weight loss rates of X80 pipeline steel under different systems are shown in Fig 7. As shown Fig 7, on day 20, the corrosion weight loss rate of X80 pipeline steel ranked as *E. coli* + 20 ppm RF system > *E. coli* system > 20 ppm RF system > blank system. This indicated that *E. coli* accelerates the X80 pipeline steel corrosion, and RF increased *E. coli*'s corrosion rate. This was because

E. coli attached to the surface of X80 pipeline steel, *E. coli* secreted Extracellular Polymeric Substances (EPS), and induced Fe chelation reaction, accelerating the corrosion of the X80 pipeline steel. The addition of RF could transfer electrons, binding distant *E. coli* into contact with the X80 pipeline steel, increasing the concentration of *E. coli* around X80 pipeline steel, leading to increased corrosion [23,24]. The corrosion weight loss rate of the 20 ppm RF system was greater than that of the blank system, probably because RF acted as an electron shuttle, promoting some corrosion reactions. This is consistent with the results of P.Y. Zhang et al. [19], where RF has less effect on the corrosion of metals.

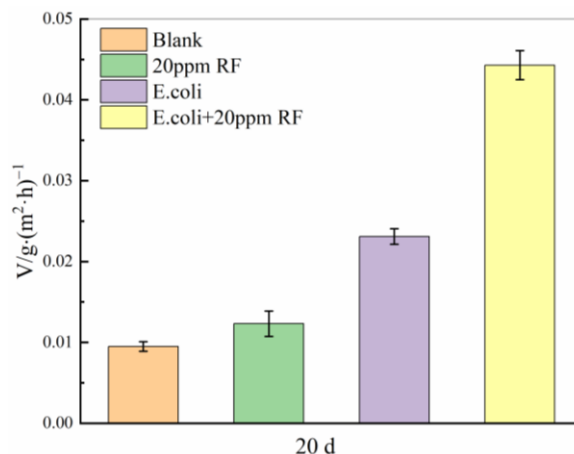


Figure 7. Corrosion weight loss rates of X80 pipeline steel in different systems (Blank, 20 ppm RF, *E. coli*, *E. coli* + 20 ppm RF)

3.3. Corrosion products analysis

As shown in Fig 8, the sparseness of corrosion products on the surface of X80 pipeline steel after 20 days of corrosion differs between systems. In the blank system (Fig 8(a)) and the 20 ppm RF system (Fig 8(b)), because there was no *E. coli*, there was no adsorption of EPS on the surface of the metal substrate. Corrosion products did not entirely cover the metal substrate surface, and the metal substrate exposed to the culture medium continued to absorb oxygen corrosion slowly. In the *E. coli* + 20 ppm RF system (Fig 8(d)), the corrosion products formed a “skeleton” structure with *E. coli*, and there were some filaments, used to connect *E. coli* and corrosion products with a similar mechanism of action and function to those of nanoconductors [25]. However, the filament generation mechanism is unclear; RF might generate it in the electron transfer between *E. coli* and the metal. Using needle-shaped products in the corrosion products, combined with the EDS analysis in Table 2, it is suspected that the corrosion product might be Fe₃O₄ or α -FeOOH. The corrosion product coverage on the X80 pipeline steel surface in the *E. coli* system (Fig 8(c)) was denser than that in the *E. coli* + 20 ppm RF system, but there were still voids in the corrosion product layer.

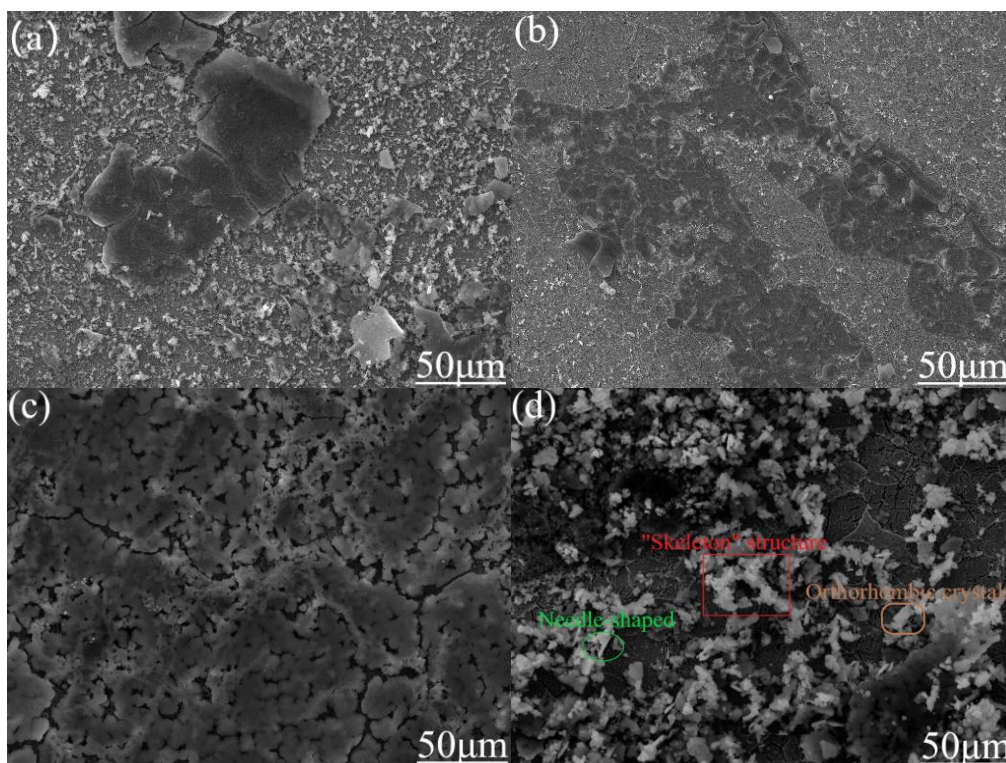
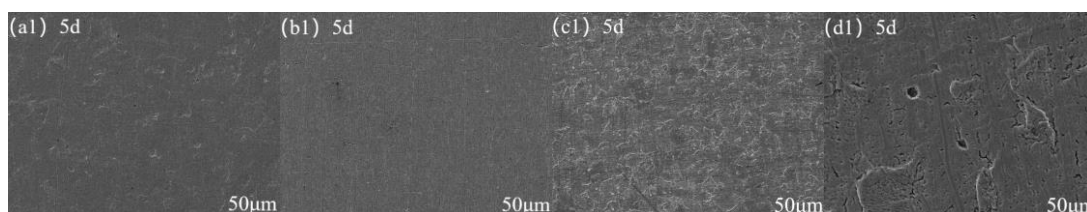


Figure 8 Surface corrosion products of X80 pipeline steel after 20 days of corrosion under different systems: (a) blank system, (b) 20 ppm RF system, (c) *E. coli* system, (d) *E. coli* + 20 ppm RF system

Table 2. Elemental content of surface corrosion products of X80 pipeline steel under different systems after 20 d

System	C/wt%	O/wt%	Fe/wt%	P/wt%
Blank	15.72	11.94	71.30	0.11
20 ppm RF	15.29	15.09	68.49	0.13
<i>E. coli</i>	8.53	30.28	59.67	0.03
<i>E. coli</i> +20 ppm RF	15.29	15.09	68.49	0.13

3.4. Corrosion morphology analysis



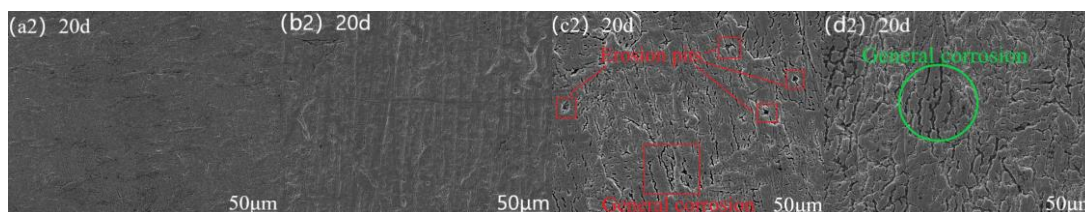


Figure 9. Microstructure of X80 pipeline steel corrosion matrix under different systems: (a1) (a2) blank system, (b1) (b2) 20 ppm RF system, (c1) (c2) *E. coli* system, (d1) (d2) *E. coli* + 20 ppm RF system

As shown in Fig 9, X80 pipeline steel has corrosion on its substrate surface in different systems. After five days in the blank system (Fig 9(a1)), X80 pipeline steel showed scattered pitting pits on the surface of the substrate, and the pitting pits were small. After 20 days (Fig 9(a2)), the pitting pits expanded and increased. After five days in the 20 ppm RF system (Fig 9(b1)), several pitting pits existed on the surface of the substrate; however, after 20 days (Fig 9(b2)), there was a tendency for general corrosion along the direction of the metal grain boundaries, leading to increased corrosion. This was mainly because, in addition to oxygen, RF promotes some corrosion, leading to increased corrosion, consistent with the corrosion weight loss rates. After five days in the *E. coli* system (Fig 9(c1)), the surface of the metal substrate had many pitting pits; after 20 days (Fig 9(c2)), the pitting pits expanded into patches, forming a general corrosion phenomenon, which destroyed the metal surface structure. After five days of soaking in the *E. coli* + 20 ppm RF system (Fig 9(d1)), the surface of X80 pipeline steel showed a slight general corrosion phenomenon. After 20 days (Fig 9(d2)), the general corrosion intensified, and cracks further expanded, producing more severe corrosion than in the *E. coli* system. This is because *E. coli* can use RF for extracellular electron transfer, which increases the *E. coli* concentration around X80 pipeline steel. RF also helps reduce Fe^{3+} oxides, thus accelerating the corrosion of X80 pipeline steel [26]. Zhang et al. also showed that RF increased the depth of metal corrosion pits [19].

3.5. Electrochemical corrosion measurements

3.5.1. Open circuit potential

As shown in Fig 10, the free-corrosion potential of the X80 pipeline steel in the blank system in the first two days showed a constant negative shift. Through, the second to the fourth day showed a positive shift, followed by a continuous negative shift phenomenon. The negative shift of the free-corrosion potential in the blank system indicates that X80 pipeline steel is protected from the corrosion process by oxygen absorption corrosion with oxygen in the medium. The above process forms corrosion products on the metal surface and prevents further oxygen diffusion, resulting in a positive shift of the free-corrosion potential after the second day. The corrosion products on the surface of X80 pipeline steel become loose and fall off with the immersion time. The formation of oxygen concentration difference

cells on the metal surface prompted X80 pipeline steel to corrode again, showing a negative to positive corrosion potential after the fourth day. The 20 ppm RF and the blank systems corrosion process were similar.

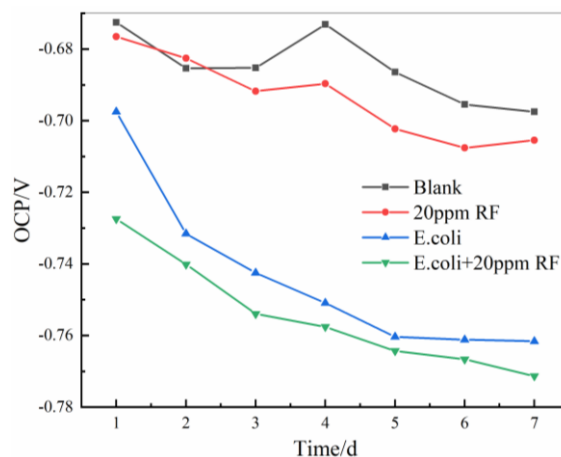


Figure 10. Variation curve of free-corrosion potential of X80 pipeline steel with time under different systems (Blank, 20 ppm RF, *E. coli*, *E. coli* + 20 ppm RF)

The free-corrosion potential of X80 pipeline steel in the *E. coli* system always showed a constant negative shift, indicating that the probability of corrosion increased with immersion time. The free-corrosion potential of X80 pipeline steel in the *E. coli* + 20 ppm RF system also showed a constant negative shift. However, compared with the *E. coli* system, its potential value was more negative. The greater the corrosion thermodynamic tendency of X80 pipeline steel, the more likely it is to cause corrosion of X80 pipeline steel [27-29]. It has been proposed that RF acts as an electron shuttle, making extracellular electron transfer easier [30].

3.5.2. EIS measurements

As shown in Fig 11, the Nyquist curves of the blank and the 20 ppm RF systems were a single capacitive arc resistance. The radius of the capacitive arc resistance increased continuously with the soaking time. The radius of capacitive arc resistance is generally proportional to the corrosion resistance of the metal; the more effective the radius of capacitive arc resistance, the better the corrosion resistance [31-33]. Therefore, the corrosion resistance of X80 pipeline steel in the blank and 20 ppm RF systems increased continuously with soaking time.

The capacitive arc radius of the *E. coli* system gradually increased in the first six days. It decreased on the seventh day, while the radius of the capacitive arc of the *E. coli* +20 ppm RF system gradually increased in the first five days and decreased on the sixth and seventh days. Roughly comparing the radius of the capacitive arc at day seven under different systems, the radius of arc the capacitive in the presence of *E. coli* was smaller than that of the sterile environment, indicating that X80

pipeline steel was more prone to corrosion in the *E. coli* environment. The radius of the *E. coli* + 20 ppm RF system's capacitive arc was smaller than the *E. coli* system, indicating that the X80 pipeline steel in the *E. coli* + 20 ppm RF system was more susceptible to corrosion than in the *E. coli* system.

The equivalent circuit diagram in Fig 12 was selected for fitting by ZsimpWin 3.5 software. The blank system and the 20 ppm RF system were fitted using the equivalent circuit diagram in Fig 12(a), and the *E. coli* system and the *E. coli* + 20 ppm RF system were fitted using the equivalent circuit diagram in Fig 12(b). In the equivalent circuit diagram, R_s is the solution resistance, R_t is the charge transfer resistance, Q_{dl} is the bilayer capacitance, Q_{bf} is the biofilm capacitance, and R_{bf} is the biofilm resistance [34,35].

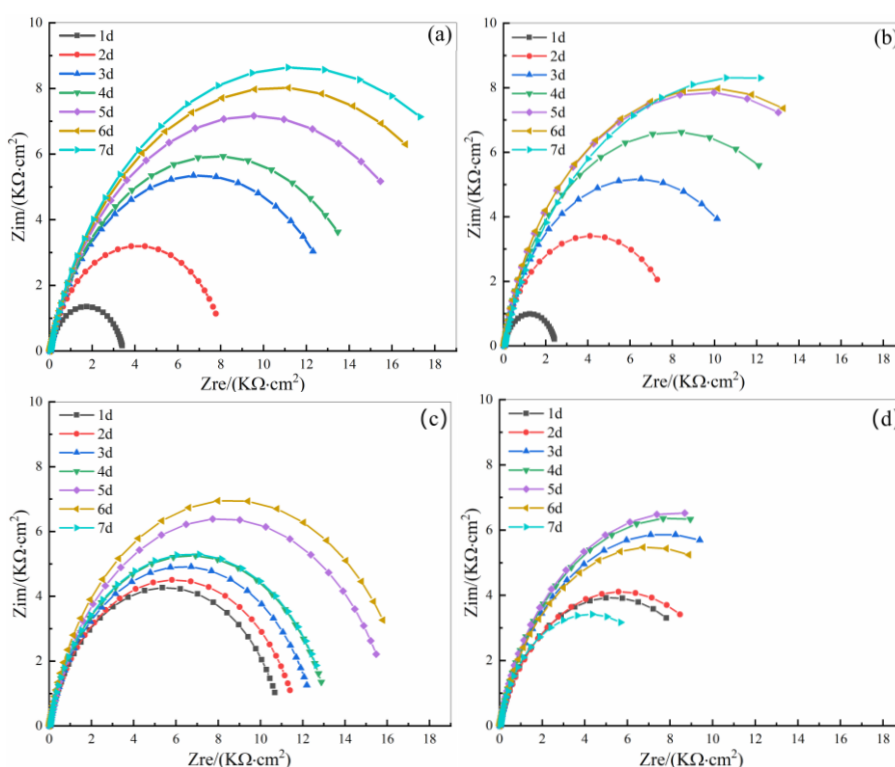


Figure 11. EIS of X80 pipeline steel corrosion for 7 days under different systems: (c) blank system, (b) 20 ppm RF system, (c) *E. coli* system, (d) *E. coli* + 20 ppm RF system

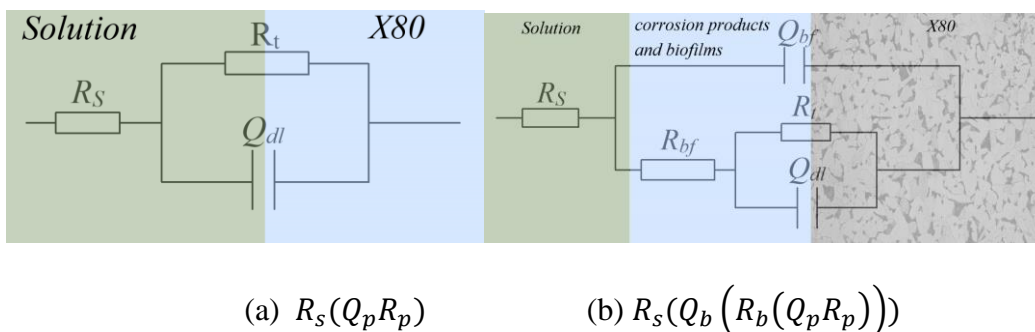


Figure 12. Equivalent circuit diagram of EIS (a) $R_s(Q_p R_p)$, (b) $R_s(Q_b (R_b (Q_p R_p)))$

As shown in Table 3, the charge transfer resistance in the blank and 20 ppm RF systems increased with the soaking time, indicating that the corrosion layer formed in the blank and 20 ppm RF systems inhibited the corrosion of the X80 pipeline steel.

As shown in Table 4, the value of charge transfer resistance R_t in the *E. coli* system gradually increased from day 1 to day 6 and decreased from day 6 to day 7, indicating that the corrosion resistance of X80 pipeline steel gradually increased in the first six days due to corrosion products and metabolites. From day 6 to day 7 with the shedding of corrosion products and biofilm rupture, a differential pool of oxygen concentration was formed on the metal surface, and the metal substrate came into contact with *E. coli*, resulting in a decrease in the corrosion resistance of X80 pipeline steel. $R_p = R_{bf} + R_t$, R_p is the polarization resistance of X80 pipeline steel during the corrosion process, R_p represent the electrochemical reaction resistance, the value of R_p^{-1} is proportional to the corrosion rate of the metal; the more significant the R_p^{-1} , the faster the corrosion rate of the metal [36,37]. The R_p value also shows that the corrosion resistance of X80 pipeline steel increased first and then decreased in the *E. coli* system. D. Wang et al. argued that the R_p data reflect 84% faster MIC in the presence of 20 ppm riboflavin at the end of the incubation [38,39], roughly the same as the results in this paper.

As shown in Table 5, the charge transfer resistance R_t value of the *E. coli* + 20 ppm RF system gradually increased from day 1 to day 3. It gradually decreased from day 4 to day 7, indicating an increase and then a decrease in the corrosion resistance of X80 pipeline steel in the *E. coli* + 20 ppm RF system. Compared with the X80 pipeline steel in the *E. coli* system, the X80 pipeline steel in the *E. coli* + 20 ppm RF system reduced corrosion resistance on the fourth day. In contrast, on the seventh day, the *E. coli* system showed a decrease in corrosion resistance, which may be related to the electron shuttle RF. Perhaps RF acts as an electron shuttle in the corrosion process, allowing easy charge transfer during corrosion.

Table 3. Parameters of the components of the equivalent circuit of the blank system and the 20ppm RF system

System	Time/d	$R_s(\Omega \cdot \text{cm}^2)$	$Q_{dl}(\mu\text{F}/\text{cm}^2)$	n_1	$R_t(\Omega \cdot \text{cm}^2)$	
Blank	1	40.47 ± 0.27	$1.63 \times 10^{-4} \pm 2.37 \times 10^{-6}$	0.86 ± 0.0037	3401 ± 34	
		33.67 ± 0.34	$1.98 \times 10^{-4} \pm 3.16 \times 10^{-6}$	0.84 ± 0.0044	8212 ± 157	
	3	33.4 ± 0.39	$1.98 \times 10^{-4} \pm 3.25 \times 10^{-6}$	0.83 ± 0.0047	13949 ± 373	
		4	34.94 ± 0.36	$1.93 \times 10^{-4} \pm 2.76 \times 10^{-6}$	0.83 ± 0.0040	15558 ± 378
	5	32.52 ± 0.34	$1.99 \times 10^{-4} \pm 2.67 \times 10^{-6}$	0.82 ± 0.0038	18963 ± 506	
		6	30.46 ± 0.3	$2.02 \times 10^{-4} \pm 2.51 \times 10^{-6}$	0.82 ± 0.0036	21314 ± 575
	7		31.15 ± 0.28	$2.07 \times 10^{-4} \pm 2.29 \times 10^{-6}$	0.82 ± 0.0032	22925 ± 584
		20 ppm RF	1	33.42 ± 0.18	$4.17 \times 10^{-4} \pm 4.86 \times 10^{-6}$	0.87 ± 0.0036

2	34.51 ± 0.29	4.15×10 ⁻⁴ ± 5.01×10 ⁻⁶	0.88 ± 0.0042	8304 ± 181
3	33.08 ± 0.23	3.86×10 ⁻⁴ ± 3.63×10 ⁻⁶	0.88 ± 0.0032	12604 ± 257
4	35.07 ± 0.23	3.64×10 ⁻⁴ ± 3.17×10 ⁻⁶	0.88 ± 0.003	16139 ± 348
5	30.44 ± 0.22	3.75×10 ⁻⁴ ± 3.16×10 ⁻⁶	0.87 ± 0.0029	19147 ± 180
6	31.93 ± 0.17	3.67×10 ⁻⁴ ± 2.61×10 ⁻⁶	0.87 ± 0.0024	19535 ± 374
7	29.38 ± 0.22	3.77×10 ⁻⁴ ± 3.37×10 ⁻⁶	0.81 ± 0.0029	21576 ± 720

Table 4. Parameters of the components of the equivalent circuit of the *E. coli* system

Time/d	$R_s/(\Omega \cdot \text{cm}^2)$	$Q_{bf}/(\mu\text{F} \cdot \text{cm}^{-2})$	n_1	$R_{bf}/(\Omega \cdot \text{cm}^2)$	$Q_{dl}/(\mu\text{F} \cdot \text{cm}^{-2})$	n_2	$R_t/(\Omega \cdot \text{cm}^2)$
1	27.35 ± 0.22	6.32×10 ⁻⁵ ± 2.59×10 ⁻⁶	0.92 ± 0.0071	4569 ± 1010	2.56×10 ⁻⁴ ± 5.53×10 ⁻⁵	0.58 ± 0.24	12090 ± 9852
2	30.83 ± 0.16	5.46×10 ⁻⁵ ± 1.61×10 ⁻⁶	0.92 ± 0.005	4339 ± 735	2.11×10 ⁻⁴ ± 2.61×10 ⁻⁵	0.58 ± 0.17	12240 ± 8845
3	26.87 ± 0.33	5.88×10 ⁻⁵ ± 3.80×10 ⁻⁶	0.92 ± 0.011	4703 ± 2048	2.13×10 ⁻⁴ ± 6.98×10 ⁻⁵	0.53 ± 0.38	16490 ± 2805
4	20.76 ± 0.21	5.74×10 ⁻⁵ ± 3.19×10 ⁻⁶	0.93 ± 0.009	3773 ± 1648	1.48×10 ⁻⁴ ± 3.75×10 ⁻⁵	0.48 ± 0.15	19320 ± 996
5	21.36 ± 0.09	6.19×10 ⁻⁵ ± 2.00×10 ⁻⁶	0.93 ± 0.005	2801 ± 90	1.08×10 ⁻⁴ ± 1.08×10 ⁻⁵	0.45 ± 0.047	27230 ± 4512
6	22.41 ± 0.15	9.92×10 ⁻⁵ ± 4.19×10 ⁻⁶	0.94 ± 0.0075	3494 ± 1383	1.13×10 ⁻⁴ ± 1.75×10 ⁻⁵	0.51 ± 0.059	29070 ± 4794
7	20.8 ± 0.15	8.67×10 ⁻⁵ ± 3.76×10 ⁻⁶	0.93 ± 0.0074	3362 ± 1027	1.30×10 ⁻⁴ ± 2.18×10 ⁻⁵	0.60 ± 0.095	13080 ± 2910

Table 5. Parameters of the components of the equivalent circuit of the *E. coli* + 20 ppm RF system

Time/d	$R_s/(\Omega \cdot \text{cm}^2)$	$Q_{bf}/(\mu\text{F} \cdot \text{cm}^{-2})$	n_1	$R_{bf}/(\Omega \cdot \text{cm}^2)$	$Q_{dl}/(\mu\text{F} \cdot \text{cm}^{-2})$	n_2	$R_t/(\Omega \cdot \text{cm}^2)$
1	17.41 ± 0.45	2.04×10 ⁻⁴ ± 1.18×10 ⁻⁵	0.51 ± 0.022	1424 ± 268	2.42×10 ⁻⁴ ± 7.32×10 ⁻⁶	0.90 ± 0.0061	16090 ± 590
2	17.2 ± 0.67	1.96×10 ⁻⁴ ± 5.7×10 ⁻⁶	0.43 ± 0.018	1340 ± 332	2.85×10 ⁻⁴ ± 1.31×10 ⁻⁵	0.89 ± 0.0045	24890 ± 179
3	16 ± 1.05	1.61×10 ⁻⁴ ± 3.22×10 ⁻⁵	0.47 ± 0.087	1402 ± 895	3.49×10 ⁻⁴ ± 3.65×10 ⁻⁵	0.90 ± 0.015	28800 ± 676
4	17.07 ± 0.31	2.27×10 ⁻⁴ ± 5.36×10 ⁻⁵	0.67 ± 0.042	1230 ± 210	3.07×10 ⁻⁴ ± 5.43×10 ⁻⁵	0.92 ± 0.017	16930 ± 490
5	20.03 ± 0.05	4.48×10 ⁻⁴ ± 9.35×10 ⁻⁶	0.90 ± 0.004	1306 ± 231	1.69×10 ⁻⁴ ± 6.73×10 ⁻⁶	0.70 ± 0.012	16280 ± 457
6	17.61 ± 0.07	4.69×10 ⁻⁴ ± 1.55×10 ⁻⁵	0.90 ± 0.007	1309 ± 256	1.96×10 ⁻⁴ ± 1.2×10 ⁻⁵	0.74 ± 0.023	16030 ± 557
7	17.74 ± 0.05	7.36×10 ⁻⁴ ± 1.48×10 ⁻⁵	0.91 ± 0.005	2068 ± 475	3.01×10 ⁻⁴ ± 3.7×10 ⁻⁵	0.73 ± 0.041	6903 ± 629

3.5.3. Polarization curves

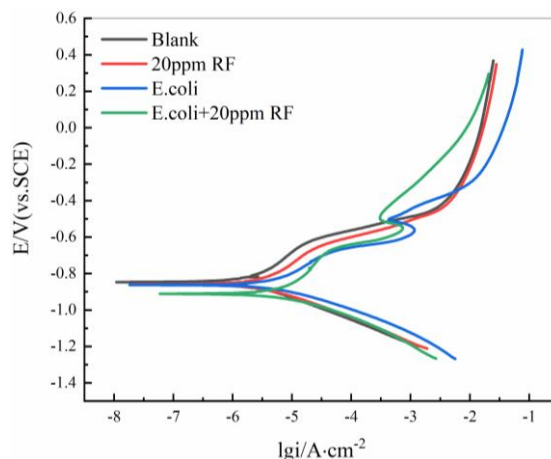


Figure 13. Corrosion polarization curves of X80 pipeline steel under different systems (Blank, 20 ppm RF, *E. coli*, *E. coli* + 20 ppm RF)

The polarization curves for 7 d corrosion of X80 pipeline steel in different systems are shown in Fig 13, and the kinetic parameters are shown in Table 6. Fig 13 shows that the polarization curves of the *E. coli* system and the *E. coli* + 20 ppm RF system were located to the lower right of the blank system and the 20 ppm RF system, indicating that X80 pipeline steel has a greater tendency to corrode in the environment where *E. coli* was present. The polarization curve of the *E. coli* + 20 ppm RF system was again located to the lower right of the *E. coli* system, indicating that X80 pipeline steel in the *E. coli* + 20ppm RF system in the corrosion tendency of the largest [40,41].

The corrosion current density of different systems was different, as shown in Table 6. The size of corrosion current density I_{corr} was *E. coli* + 20 ppm RF system > *E. coli* system > 20 ppm RF system > blank system. According to Faraday’s law, the corrosion rate positively correlates with the corrosion current density, so the corrosion of X80 pipeline steel in *E. coli* + 20 ppm RF system was the most serious. Consistent with the corrosion weight loss rate, open circuit potential, and EIS measurements. Meanwhile, the electrochemical test results are consistent with R. Jia et al. [42,43], showing that adding RF promotes microbial corrosion of metals.

Table 6. Polarization curve fitting results

	$\beta_a/(mv)$	$\beta_c/(mv)$	$E_{corr}/(VS.SCE)$	$I_{corr}/(A \cdot cm^{-2})$
Blank	279	136	-0.846	2.68×10^{-6}
20ppm RF	203	111	-0.861	2.78×10^{-6}
<i>E. coli</i>	233	110	-0.863	6.15×10^{-6}
<i>E. coli</i> + 20ppm RF	392	121	-0.911	9.50×10^{-6}

3.5.4. Analysis of corrosion products

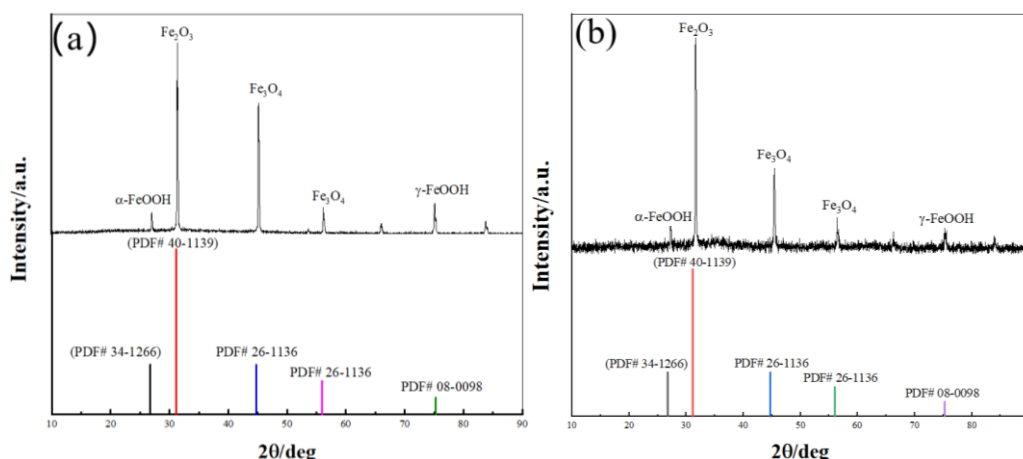
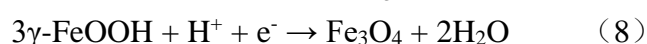
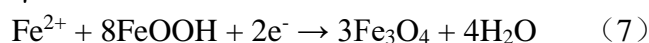
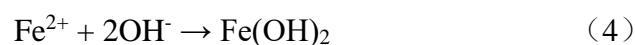
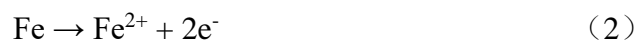


Figure 14. XRD test results for X80 pipeline steel surface corrosion products:(a) *E. coli* system, (b) *E. coli* + 20 ppm RF

Fig 14 shows that the surface corrosion products of X80 pipeline steel in the *E. coli* and *E. coli* + 20 ppm RF systems had the same composition, mainly including α -FeOOH, Fe_2O_3 , Fe_3O_4 , and γ -FeOOH. It indicated that the electron shuttle RF did not change the corrosion path of *E. coli* on X80 pipeline steel. The corrosion process of X80 pipeline steel in the *E. coli* and *E. coli* + 20 ppm RF systems is mainly due to Fe^{2+} (2) precipitated by the Fe oxidation reaction at the anode and the oxygen corrosion reaction of iron (3) (4) at the cathode. The $\text{Fe}(\text{OH})_2$ generated by the corrosion process was then converted to trivalent iron oxides (5) due to its instability (6), and the XRD results also confirmed α -FeOOH and γ -FeOOH in corrosion products. The γ -FeOOH generated in the *E. coli* system further reacted with the dissolved Fe^{2+} at the anode to form Fe_3O_4 (7). The electrons released from the dissolution of anodic iron in the *E. coli* + 20 ppm RF system and the electrons generated from the metabolic activity of *E. coli* were transferred to γ -FeOOH through RF to reduce it (8) to produce Fe_3O_4 . The corrosion process is shown in Fig 15. The corrosion process of X80 pipeline steel and XRD tests combined with electrochemical tests show that the system's charge transfer resistance under RF decreases, and the corrosion products were layered. However, the corrosion product composition was the same, indicating that RF only affected the corrosion process of *E. coli*. This is consistent with the conclusion of D. Wang et al. [38], showing that the presence of riboflavin does not alter the corrosion mechanism.



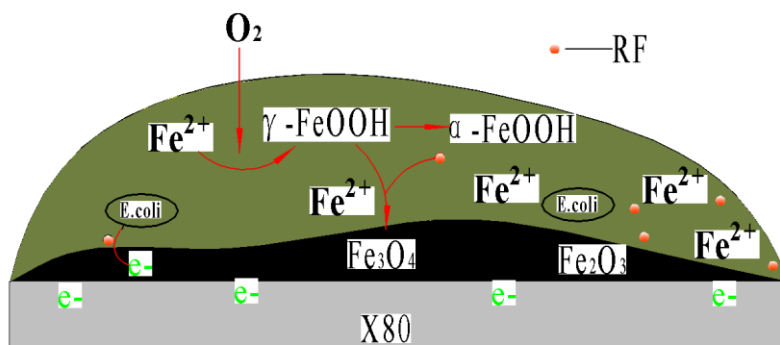


Figure 15. Corrosion process mechanism diagram

4. CONCLUSION

In this paper, we investigated the effect of RF on the corrosion of X80 pipeline steel *E. coli* by adding 20ppm RF to make *E. coli* available for extracellular electron transfer. The main findings of the study are as follows:

(1) The CV test showed that the *E. coli* bacterium and metabolites were not electro-active. At the same time, the oxidation peak of the *E. coli* + 20 ppm RF system was -0.489 V (vs. SCE), and the reduction peak was -0.401 V (vs. SCE), indicating that RF was involved in the electron transfer between *E. coli* and the electrode. Moreover, the electrochemical transformation of RF was under Randles Sevcik's controlled diffusion-reaction formula, which was diffusion controlled.

(2) The corrosion rate test results showed that the corrosion weight loss rate under the *E. coli* + 20 ppm RF system was twice that of the *E. coli* system, indicating that the electron shuttle RF had a facilitating effect on the corrosion of the X80 pipeline steel *E. coli*.

(3) The electrochemical and XRD tests showed that 20 ppm RF caused electron transfer between *E. coli* and corrosion products, resulting in the layering of corrosion products, and promoting the conversion of the outer to the inner corrosion products. The corrosion products of the *E. coli* system and *E. coli* + 20 ppm RF system had the same composition. However, they contained different proportions, which indicated that the addition of RF did not change the corrosion pathway of *E. coli*.

ACKNOWLEDGMENTS

This project is supported financially supported by the National Nature Science Foundation of China(No. 52171062), 2021 Open Project of Failure Mechanics and Engineering Disaster Prevention, Key Lab of Sichuan Province(No. FMEDP202109), The Opening Foundation of Sichuan Province Engineering Center for Powder Metallurgy (No.SC-FMYJ2019-07), Talent Introduction Project of Sichuan University of Science and Engineering (No. 2020RC19), the Project of Sichuan Provincial Key Lab of Process Equipment and Control (GK201912, GK202004, GK202204) and The undergraduate innovation and business startups training program of SUSE (No. CX2020012).

COMPETING INTERESTS

The authors have no relevant financial or non-financial interests to disclose.

CONSENT FOR PUBLICATION

All authors consent to the publication of the manuscript.

AUTHOR CONTRIBUTIONS

Conceived or designed: Shisen Yan, LI Lin, Jieshuang Mu, Yanbing Guan. Performed research: Shisen Yan, Sheng Lai. Analyzed data: Shisen Yan, Mingxing Tan. Wrote the paper: Shisen Yan. Revising the manuscript: Lei FU, Yingqian Zhang, Zhengguo Wang.

References

1. S.Y. Li, Y.G. Kim, K.S. Jeon, Y.T. Kho and T. Kang, *Corrosion*, 57(2001) 815.
2. X. Chen, X.G. Li, C.W. Du and Y.F. Cheng, *Corros. Sci.*, 51(2009) 2242.
3. J.H. Luo, C.M. Xu and D.P.Y., *Journal of Chinese Society for Corrosion and protection*, 36(2016) 321.
4. T.Q. Wu, M.C. Yan, J. Xu, C. Sun, D.C. Zeng, C.K. Yu and W. Ke, *Journal of Materials Science & Technology*, 31(2015) 413.
5. T.L. Skovhus, R.B. Eckert and E. Rodrigues, *J. Biotechnol.*, 256(2017) 31.
6. L.M. Gieg, T.R. Jack and J.M. Foght, *Appl. Microbiol. Biotechnol.*, 92(2011) 263.
7. D. Wang, J. Liu, R. Jia, W. Dou, S. Kumseranee, S. Punpruk and T. Gu, *Corros. Sci.*, 177(2020) 108993.
8. Y.X. Fan, C.Y. Chen, Y.X. Zhang, H.X. Liu, H.W. Liu and H.F. Liu, *Bioelectrochemistry*, 141(2021) 107880.
9. M. Masuda, S. Freguia, Y.F. Wang, S. Tsujimura and K. Kano, *Bioelectrochemistry*, 78(2010) 173.
10. S.A. Wade, M.A. Javed, E.A. Palombo, S.L. McArthur and P.R. Stoddart, *Int. Biodeterior. Biodegrad.*, 121(2017) 97.
11. Y.P. Diao, L.C. Yan and K.W. Gao, *Mater. Des.*, 198(2021) 109326.
12. R. Jia, J.L. Tan, P. Jin, D.J. Blackwood, D. Xu and T.Y. Gu, *Corros. Sci.*, 130(2018) 1.
13. T. Gu, R. Jia, T. Unsal and D. Xu, *Journal of Materials Science & Technology*, 34(2019) 631.
14. M. Rosenbaum, F. Aulenta, M. Villano and L.T. Angenent, *Bioresour. Technol.*, 102(2011) 324.
15. Y. Li, D. Xu, C. Chen, X. Li, R. Jia, D. Zhang, T. Gu, *Journal of Materials Science & Technology*, 34(2018) 1713.
16. R. Jia, T. Unsal, D. Xu, Y. Leckbach and T. Gu, *Int. Biodeterior. Biodegrad.*, 137(2019) 42.
17. D. Xu, T. Gu, *Int. Biodeterior. Biodegrad.*, 91(2014) 74.
18. M. Zhou, H. Wang, D.J. Hassett and T. Gu, *J. Chem. Technol. Biotechnol.*, 88(2013) 508.
19. P. Zhang, D. Xu, Y. Li, K. Yang and T. Gu, *Bioelectrochemistry*, 101(2015) 14.
20. F. Guan, Z. Liu, X. Dong, X. Zhai, B. Zhang, J. Duan and B. Hou, *Sci. Total Environ.*, 788(2021) 147573.
21. W. Chen, X.Y. Liu, C. Qian, X.N. Song, W.W. Li and H.Q. Yu, *Biosens. Bioelectron.*, 64(2015) 25.
22. Y. Wu, F. Li, T. Liu, R. Han and X. Luo, *Electrochim. Acta*, 213(2016) 408.
23. R. Jia, D. Wang, P. Jin, T. Unsal, D.Q. Yang, J.K. Yang, D. Xu, T.Y. Gu, *Corros. Sci.*, 153(2019) 127.
24. E. Lojou, M.T. Giudici-Ortoni and P. Bianco, *J. Electroanal. Chem.*, 579(2005) 199.
25. H. Li, D. Xu, Y. Li, H. Feng, Z. Liu, X. Li and K. Yang, *PloS One*, 10(2015) e0136183.
26. Y. Yuan, L. Zhou, R. Hou, Y. Wang and S. Zhou, *Trends Biotechnol.*, 39(2021) 181.
27. Q. Fan, L. Fu, L. Lin, S. Lai, X.J. Huang, Y.Q. Zhang, Y.R. Luo, X.L. Li and H. Z. Zhang, *Int. J. Electrochem. Sci.*, 16(2021) 9.
28. L. Lin, C. Liu, L. Fu, Y. Zeng, M. Gong, X.J. Cui, J.C. Meng and X.J. Huang, *Int. J. Electrochem. Sci.*, 16(2021) 6.
29. X.J. Huang, L. Fu, L. Lin, S. Lai, Q. Fan, Y.Q. Zhang, X.L. Li and C. Liu, *Mater. Res. Express*, 8(2021) 106526.
30. S. Baeza, N. Vejar, M. Gulppi, M. Azocar, F. Melo, A. Monsalve and M.A. Páez, *Corros. Sci.*,

- 67(2013) 32.
31. H.B. Li, E. Zhou, Y.B. Ren, D.W. Zhang, D. Xu, C.G. Yang, H. Feng, Z.H. Jiang, X.G. Li, T.Y. Gu and K. Yang, *Corros. Sci.*,111(2016) 811.
 32. L.B. Yu, M.C. Yan, J. Ma, M.H. Wu, Y. Shu, C. Sun, J. Xu, C.K. Yu and Y.C. Qing, *Acta Metall. Sinica*, 53(2017) 1568.
 33. J.E.G. Gonzalez, A.F.J.H. Santana and J.C. Mirza-rosca, *Corros. Sci.*,40(1998) 2141.
 34. J.L. Wang, F.P. Xiong, H.W. Liu, T.S. Zhang, Y.Y. Li, C.J. Li, W. Xia, H.T. Wang and H.F. Liu, *Bioelectrochemistry*, 129(2019) 10.
 35. P.B. Raja, M. Fadaeinasab, A.K. Qureshi, A.A. Rahim, H. Osman, M. Litaudon and K. Awang, *Industrial & Engineering Chemistry Research*, 52(2013) 10582.
 36. J.A. Gralnick and D.K. Newman, *Mol. Microbiol.*, 65(2007) 1.
 37. D. Xu, Y.C. Li, F.M. Song and T.Y. Gu, *Corros. Sci.*,77(2013) 385.
 38. D. Wang, P. Kijkla, M. Mohamed, M.E., M.A. Saleh, S. Kumseranee, S. Punpruk and T. Gu, *Bioelectrochemistry*, 142(2021) 107920.
 39. T. Gu, D. Wang, Y. Lekbach and D. Xu, *Current Opinion Electrochemistry*, 29(2021) 100763.
 40. F. Xie, X.F. Yang, D. Wang and Y.B. Wang, J. Qi and H.Q. Feng, *Materials for Mechanical Engineering*, 39(2015) 59.
 41. W.J. Xie, D. Li, Y.L. Hu, B.L. Guo and J.Z. Zhang, *Journal of Chinese Society Corrosion and Protection*, 19(1999) 95.
 42. R. Jia, D. Yang, D. Xu and T. Gu, *Bioelectrochemistry*, 118(2017) 38.
 43. N.J. Kotloski, J.A. Gralnick, *MBio*, 4(2013) e00553.